Spatially Resolved Measurements of 3D Cellular Structure of Premixed $H_2/O_2/N_2$ Flames on a Porous-Plug Burner

Zeyu Yan, Xiangyu Nie, Shengkai Wang*
SKLTCS, CAPT, College of Engineering, Peking University
5 Yiheyuan Road, Haidian District, Beijing, 100871, China

1 Introduction

The use of hydrogen as a carbon-free chemical energy carrier has attracted extensive research attention due to its versatility, high specific energy, and non-toxic, clean nature [1]. As the majority of current power generation, aviation, and industrial heating processes rely heavily on thermochemical energy conversion strategies (such as combustion), replacing conventional fossil fuels with hydrogen would enable a substantial reduction in emissions, an improvement in efficiency, and an increase in operational flexibility [2]. However, hydrogen possesses thermodynamic, kinetic, and transport properties that are drastically different from those of conventional fuels, which can lead to intrinsic flame instabilities, especially under fuel-lean conditions [3, 4]. Of particular interest to the present study is the diffusive-thermal instability of hydrogen combustion, a phenomenon observed in off-stoichiometric hydrogen flames where an imbalance between heat and mass transport occurs. Under fuel-lean conditions, where the effective Lewis number is less than unity, this instability manifests as cellular flame fronts containing striped quenching patterns, which play an important role in dynamic extinction and re-ignition processes [7]. This, in turn, modifies the flame structure and propagation dynamics, posing challenges to the adaptation of hydrogen fuel in existing combustion facilities optimized for hydrocarbon fuels. A comprehensive understanding of the cellular instability of hydrogen flames is thus critically needed for the adjustment of combustion devices and processes for hydrogen-based fuels.

Historically, experimental studies on the cellular instability of flames have relied heavily on phenomenological observations, such as cinematographic recordings of flame morphology variations [6, 7] and chemiluminescence imaging of reaction zones [8, 9], while quantitative measurements have been relatively scarce. The use of planar laser-induced fluorescence (PLIF) to image the cross-sectional structures of cellular flames has also been reported [10], but fully resolved 3D measurements are still lacking. Since cellular flame instability is largely governed by transport processes across different scales, it is desirable to quantify relevant properties in a spatially resolved manner. Additionally, previous studies have primarily focused on premixed flames of fuel-air mixtures, where the volumetric heat release rates were relatively low. Flames with enriched or pure oxygen as the oxidizer are expected to exhibit substantially different instability boundaries and flame structures, but systematic characterization is still lacking.

To address these issues, the objective of the current study is two-fold: (a) to extend the existing diagnostic capabilities to capture the 3D distributions of key scalar fields (for example, OH radicals and gas

Correspondence to: sk.wang@pku.edu.cn

temperature) in hydrogen flames subject to cellular instability, and (b) to conduct parametric measurements on hydrogen flames to investigate the relationship between the morphology of the cellular flame front and the global flame conditions, specifically the equivalence ratio and dilution factor.

2 Experimental Method

Flame experiments were conducted on a custom-built McKenna-type axial symmetric porous-plug burner, as shown in Fig. 1. The porous-plug burner generated a relatively uniform incoming flow, thereby eliminating the effects of strain rate on the onset of flame instability. The heat loss across the burner surface also helped to stabilize the cellular structure and rendered it time-independent, thereby enabling detailed measurement over extended period of time. Similar porous-plug burners have been utilized in previous experimental studies on the premixed flame cellular instability of other fuels, such as CH_4 [11] and n-C_4H_{10} [10]. The burner used in the current study featured an 18-mm-diameter sintered bronze plug that was water-cooled to maintain a stable temperature. The temperature of the porous plug was continuously monitored using an embedded K-type thermocouple (Omega TJ36-CAXL-020-12). High-purity fuel (99.99%-grade H_2), O_2 (99.999%-grade), and N_2 (99.999%-grade) were supplied to the bottom of the burner, where they were thoroughly mixed by an in-line static mixer before passing through the porous plug. The flow rates of H_2, O_2, and N_2 were precisely controlled by three Alicat MC series mass flow controllers, with typical uncertainties of 0.1%, 0.2%, and 0.5%, respectively.

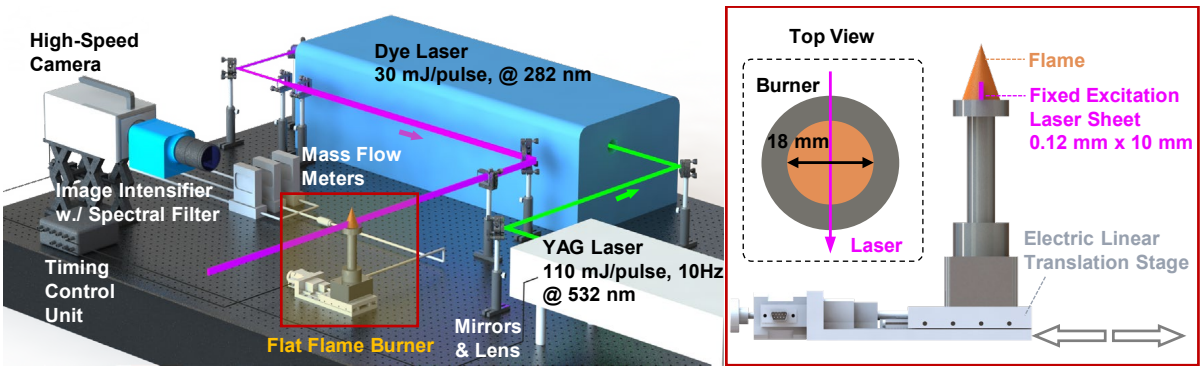

Figure 1: Schematic of the current experimental setup.

Spatially resolved measurements of the cellular flame structure were performed using OH-PLIF, where the A-X (1,0) P(13.5) and R(10.5) transitions of OH radicals at 282 nm were excited by a ns-pulsed dye laser (LIOP-TEC LIOPSTAR-N) at a repetition rate of 10 Hz. The use of two transitions allowed for quantitative determination of gas temperature from their intensity ratio, as demonstrated in a previous study by the authors [12]. The dye laser was optically pumped by a frequency-doubled pulsed Nd:YAG laser at 532 nm (InnoLas, SpitLight2000-10) to generate coherent radiation at 566 nm, which was then passed through a frequency-doubling module to produce 30-mJ laser pulses at 282 nm. The pulse energy was measured by a laser power meter (Newport Model 843-R) with less than 5% uncertainty. The excitation laser beam was expanded by three cylindrical fused silica lenses (with focal lengths of -25 mm, 500 mm and 500 mm, respectively) into a sheet of 10 mm height and 0.12 mm thickness (2-σ value). The OH-PILF signal was bandpass-filtered at 310 ± 10 nm before being collected by an image intensifier (supplied by EyeiTS, Intelligent Scientific Systems Co., LTD.) and recorded by a Phantom v611 high-speed digital camera at a pixel resolution of 256 × 512. The physical resolution of an individual pixel was determined to be 88 μm × 88 μm using a geometry calibration target.

To fully resolve the 3D cellular structure, a linear sweep of the excitation laser sheet across the hydrogen flame was performed. Specifically, the porous burner was placed on an electrically driven linear trans-

lation stage that moved continuously at a speed of 1 mm/s during each measurement, while the absolute position of the laser sheet remained unchanged. The motion of the porous burner was synchronized with the excitation laser, image intensifier, and high-speed camera using a central timing unit. The exposure time of the intensified camera was set to be 10 ns – long enough to cover the pulse width of the laser and short enough to minimize the influence of background emission. The intensifier gain was adjusted to yield a maximum pixel value of about 75% of the camera full range, in order to avoid saturation effects. The normalized distribution of OH concentration was calculated from the OH-PLIF signal by properly accounting for the effects of fluorescence quenching using a comprehensive model [13] and the spatial distribution of the excitation laser intensity through an acetone calibration experiment.

3 Results and Discussion

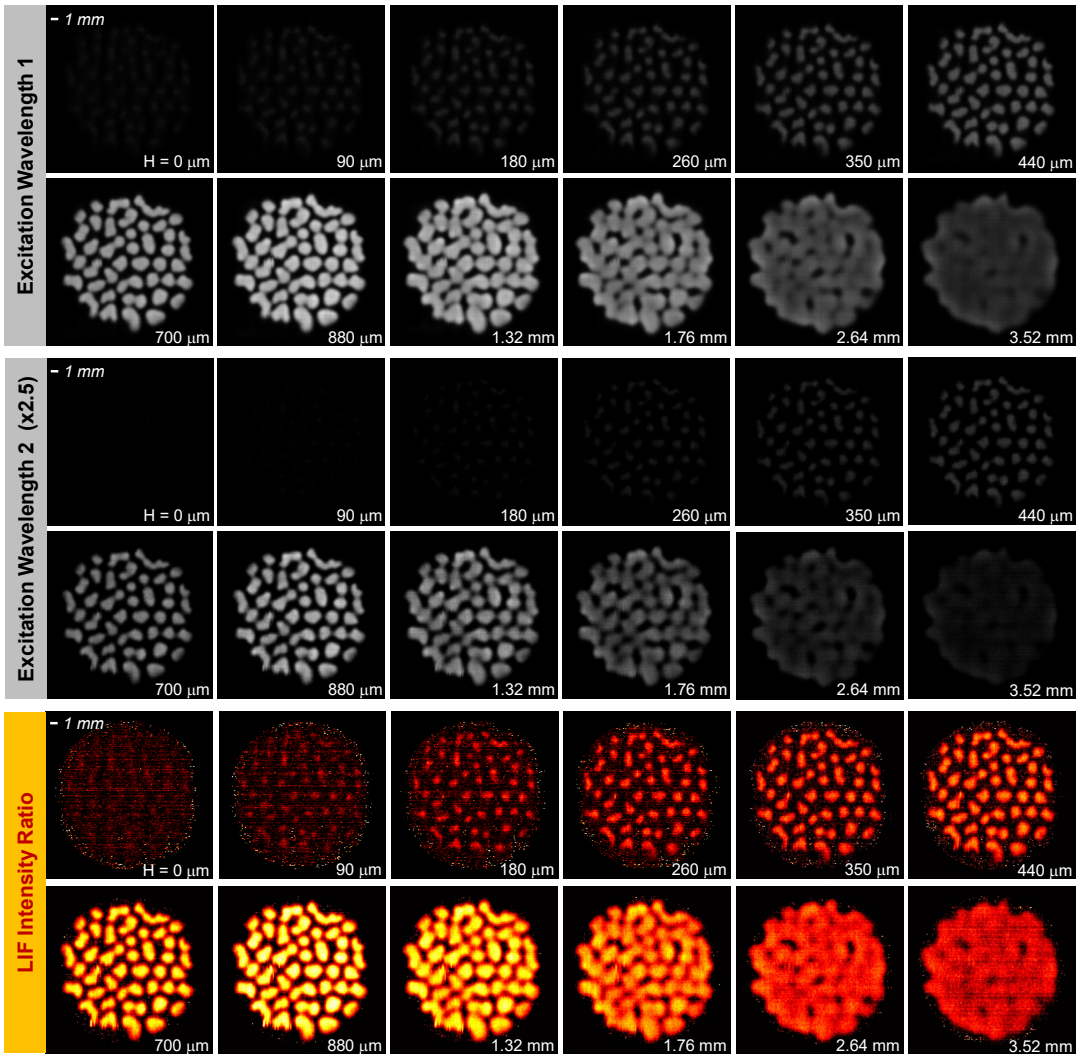

Figure 2: Representative measurement results of a cellular hydrogen flame under the conditions of $\dot{m}_{H_2}$ = 0.90 SLPM, $\dot{m}_{O_2}$ = 1.70 SLPM, and $\dot{m}_{N_2}$ = 4.70 SLPM. Shown in the top, middle, and bottom panels are the horizontal distributions of OH-PLIF intensity under P(13.5) excitation, R(10.5) excitation, and their intensity ratio, respectively, at different heights above the burner (HAB).

Fig. 1 shows the results of a representative measurement of a lean hydrogen flame at an equivalence ratio

(ϕ) of 0.265 and a dilution factor (η, defined as $\dot{m}_{H_2}/(\dot{m}_{H_2} + \dot{m}_{N_2})$) of 0.161. Note that these results correspond to horizontal slices of the 3D cellular flame, which were reconstructed from vertical slices obtained directly from the linear translation measurements. The sharpness and high contrast of these images indicate the high quality of the current data. Based on these data, quantitative determination of the spatial distributions of OH radical and gas temperature can be achieved.

Individual cells or pockets of hot combustion product were clearly observed near the burner surface, which merged further downstream of the flame at HAB above 3.5 mm, indicating that the flame front was wrinkled by diffusive-thermal instability into a 3D structure with tips extended to the close proximity of the burner surface. The burner surface was maintained at a constant temperature of 295 K throughout the experiment, which acted as a hint sink that reduced the local flame speed near the extruding tips and stabilized the cellular flame. The detailed structure was the result of balance between (a) local flame acceleration/deceleration due to differential diffusion of mass and heat, (b) local flame acceleration/deceleration induced by curvature or stretch (the Markstein lengths of lean hydrogen flames were found to be negative [14], meaning that positive flame stretch would reduce the flame speed), and (c) flame deceleration induced by heat loss to the burner surface (which scaled with the vertical gradient of local gas temperature at the surface). Under the particular conditions of Fig. 1, the dominant scales of the cell structure (both horizontal and vertical) were found to be on the order of 2 mm. The average flame height above the burner, defined by the maximum total OH PLIF intensity under P(13.5) excitation across the horizontal plane, was found to be approximately 0.9 mm.

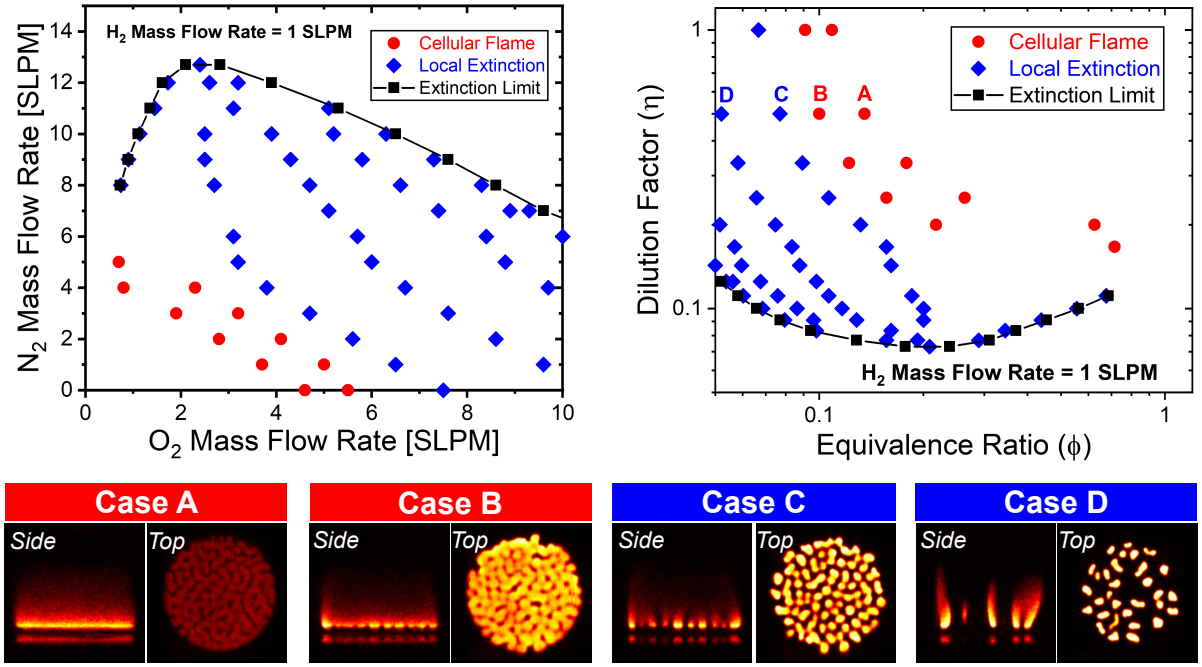

Figure 3: Regime diagram of cellular flame morphology at $\dot{m}_{H_2}$ = 1.00 SLPM. The red symbols represent cases where the flame front was distorted by a weak cellular structure but still continuous. The blue symbols represent cases where strong cellular instability led to local flame extinction and discontinuous flame fronts. The black line and symbols indicate the observed limit of total flame extinction.

A total of 65 cellular flame experiments were conducted at a fixed H_2 mass flow rate of 1.00 SLPM and varying equivalence ratios and dilution factors, the results of which are summarized in Fig. 3. Cellular instability appeared at sufficiently low equivalence ratios where the effective Lewis number (Le) of the reactive mixture was sufficiently lower than 1. For H_2/O_2 flames, the critical equivalence ratio (ϕ_{crit}) corresponding to the onset of cellular instability was found to be between 0.1 and 0.2. This value was

seen to increase with the amount of nitrogen dilution; for example, at a dilution factor of η = 0.2, ϕ_{crit} was between 0.6 and 0.7. The observed negative dependence of ϕ_{crit} on η agreed qualitatively with linear stability theory, which states that the criterion of cellular instability onset is $\mathrm{Ze}(1-\mathrm{Le}) > 2$ [15], where Ze is the Zeldovich number or non-dimensional activation energy of the reactive mixture scaling with the reciprocal of the burnt gas temperature. At higher levels of dilution, the burnt gas temperature decreases, leading to a larger value of Ze and, consequently, a larger value of ϕ_{crit}.

For a fixed dilution factor, the morphology of the cellular flame varied from small cells to large cells and transitioned from a continuous flame front with cusps to broken or isolated flame fronts exhibiting strong local extinction as the equivalence ratio decreased (see Cases A-D in Fig. 3). Similar trend was observed for flames of decreasing dilution factors and a fixed equivalence ratio, although at sufficiently low equivalence ratios ($\phi < 0.09$), all flames were seen to exhibit local extinction. Quantitative analysis of the dependence of cell size statistics on flame conditions is currently in progress.

At sufficiently high levels of dilution, total extinction or blow-off of the hydrogen flame occurred, as represented by the black line and symbols in Fig. 3. A total of 20 experiments were conducted at an H_2 mass flow rate of 1.00 SLPM, with the N_2 mass flow rate finely adjusted to determine the extinction limit. The resulting extinction boundary exhibited non-monotonic behavior, with a minimum value of $\eta = 0.073$ occurring at $\phi \approx 0.2$. Extended measurements at different H_2 mass flow rates are anticipated.

4 Conclusions

In the current study, spatially resolved multi-field measurements of the 3D cellular structure of premixed $H_2/O_2/N_2$ flames on a porous-plug burner were achieved using a unique combination of linear translation of the burner and multi-wavelength OH-PLIF. A series of parametric experiments was conducted to investigate the relationship between the morphology of the cellular flame front and the global flame conditions, specifically the equivalence ratio and dilution factor. A regime diagram of cellular flame morphology was obtained at an H_2 mass flow rate of 1.00 SLPM. The critical equivalence ratio for the onset of cellular instability, estimated from the current data, was observed to increase as the level of dilution increased. For a fixed dilution factor, the morphology of the cellular flame varied from small cells to large cells and from continuous to discontinuous as the equivalence ratio decreased. The boundary of total flame extinction was also determined. The comprehensive data on the hydrogen flame cellular structure obtained in this study should prove useful in advancing fundamental flame instability theories and providing validation targets for high-fidelity numerical combustion models.

References

[1] Pitsch H. (2024). The transition to sustainable combustion: Hydrogen-and carbon-based future fuels and methods for dealing with their challenges. Proc. Combust. Inst. 40: 105638.

[2] Verhelst S, Wallner T. (2009). Hydrogen-fueled internal combustion engines. Prog. Energy Combust. Sci. 35: 490-527.

[3] Matalon M. (2007). Intrinsic flame instabilities in premixed and nonpremixed combustion. Annu. Rev. Fluid Mech. 39: 163-191.

[4] Sánchez AL, Williams FA. (2014). Recent advances in understanding of flammability characteristics of hydrogen. Prog. Energy Combust. Sci. 41: 1-55.

[5] Robert E, Monkewitz PA. (2012). Thermal-diffusive instabilities in unstretched, planar diffusion flames. Combust. flame. 159: 1228-1238.

[6] Chen RH, Mitchell GB, Ronney PD. (1992). Diffusive-thermal instability and flame extinction in nonpremixed combustion. Proc. Combust. Inst. 24: 213-221.

[7] Robert E, Monkewitz PA. (2012). Thermal-diffusive instabilities in unstretched, planar diffusion flames. Combust. Flame. 159: 1228-1238.

[8] Antar E, Delavande J, Robert E. (2023). Experimental characterization of diffusive-thermal instabilities in CO2-diluted H2/CH4/CO unstrained diffusion flames. Combust. Flame. 250: 112636.

[9] Antar E, Robert E. (2024). Diffusive-thermal instabilities in unstrained H2O-diluted syngas diffusion flames. Combust. Flame. 261: 113313.

[10] Jiang L, Gu C, Zhou G, Li F, Wang Q. (2020). Cellular instabilities of n-butane/air flat flames probing by PLIF-OH and PLIF-CH2O laser diagnosis. Exp. Therm. Fluid Sci. 118: 110155.

[11] Konnov AA, Dyakov IV. (2005). Measurement of propagation speeds in adiabatic cellular premixed flames of CH4+ O2+ CO2. Exp. Therm. Fluid Sci. 29: 901-907.

[12] Wang S, Hanson RK. (2019). Quantitative 2-D OH thermometry using spectrally resolved planar laser-induced fluorescence. Opt. Lett. 44: 578-581.

[13] Yan Z, Wang S. (2025). StaR-LIF: State-resolved laser-induced fluorescence modeling for diatomic molecules. J. Quant. Spectrosc. Radiat. Transf. 330: 109230.

[14] Aung KT, Hassan MI, Faeth GM. (1997). Flame stretch interactions of laminar premixed hydrogen/air flames at normal temperature and pressure. Combust. Flame. 109: 1-24.

[15] Clavin P, Searby G. (2016). Combustion waves and fronts in flows: flames, shocks, detonations, ablation fronts and explosion of stars. Cambridge University Press.